Pressure and strain dependence of the strength of sintered polycrystalline Mg_2SiO_4 ringwoodite

Norimasa Nishiyama,[1] Yanbin Wang,[1] Takeyuki Uchida,[1] Tetsuo Irifune,[2] Mark L. Rivers,[1] and Steve R. Sutton[1]

[1] Differential stresses in a cylindrical rock of polycrystalline Mg_2SiO_4 ringwoodite were measured at room temperature with pressures up to 10 GPa, axial strains in excess of 20%, and strain rates between 5×10^{-5} and 4×10^{-6} s^{-1}, using the deformation-DIA coupled with monochromatic X-rays. The sample exhibited ductile behavior in axial shortening-lengthening cycles with reproducible hysteresis loops, yielding multiple well-defined stress-strain curves. Significant strain hardening was observed beyond the yield point, which occurs at axial strains around 1.5%. Large discrepancies in strength data on ringwoodite reported in previous studies, where no strain information could be obtained, can be reconciled by the strain hardening behavior. Above 8% axial strain, sample stresses reach saturation and the deformation reaches steady state, during which process the ultimate strength increases with hydrostatic pressure but are insensitive to strain rate, suggesting that the sample deforms in low-temperature plasticity regime. **Citation:** Nishiyama, N., Y. Wang, T. Uchida, T. Irifune, M. L. Rivers, and S. R. Sutton (2005), Pressure and strain dependence of the strength of sintered polycrystalline Mg_2SiO_4 ringwoodite, *Geophys. Res. Lett.*, *32*, L04307, doi:10.1029/2004GL022141.

1. Introduction

[2] Ringwoodite is a high pressure polymorph of olivine stable between 520 and 670 km depths and considered to be one of the most abundant minerals in both the subducting slabs and the surrounding mantle in this part of the mantle transition zone [e.g., *Irifune and Ringwood*, 1987]. Rheological properties of olivine and its polymorphs wadsleyite and ringwoodite play a fundamental role in subduction processes that control the dynamics of the whole mantle. Several attempts were made to investigate the rheological properties of ringwoodite. Differential stresses in polycrystalline ringwoodite were measured under high pressures both at room temperature [*Meade and Jeanloz*, 1990; *Kavner and Duffy*, 2001] and high temperature [*Chen et al.*, 1998]. These studies, carried out using different experimental techniques, show large discrepancies in reported yield strength [e.g., see *Kavner and Duffy*, 2001]. Nevertheless, all agree that ringwoodite has greater strength than olivine. *Karato et al.* [1998] deformed iron-bearing ringwoodite within its stability field and showed that relatively large grained samples

exhibited microstructure associated with dislocation creep, whereas fine-grained samples showed evidence for diffusion creep or superplasticity. *Wenk et al.* [2004] made in-situ observation of texture development in ringwoodite in the diamond anvil cell (DAC) and determined active slip systems responsible for the observed fabric.

[3] All of these studies were limited to measuring stresses only. Sample strain, a critical parameter describing the ability to flow, was not determined. As a result, there has been no quantitative mechanical data on ringwoodite describing relations between differential stress and strain at a prescribed hydrostatic pressure, temperature, and strain rate. Such mechanical data are indispensable in the determination of flow laws. As a first step towards quantitative stress-strain determination for ringwoodite, we report high-pressure, room-temperature stress-strain curves for a pre-sintered polycrystalline ringwoodite, using a deformation-DIA (D-DIA) and monochromatic X-rays [*Uchida et al.*, 2004]. These results are used to reconcile the large discrepancies in the strength of ringwoodite previously reported.

2. Experimental

[4] The deformation experiment was performed at the GSECARS 13-BM-D beamline (Advanced Photon Source) using D-DIA with monochromatic diffraction (wavelength 0.191 Å) and a radiographic imaging system (see details in work by *Wang et al.* [2003] and *Uchida et al.* [2004]).

[5] We used four sintered cubic boron nitride (cBN) anvils with truncated edge length (TEL) of 3 mm. These X-ray transparent anvils permitted observation of diffraction Debye rings over the entire 360° detector azimuth range, perpendicular to the incident beam direction. Two-dimensional (2-D) diffraction patterns were collected using an X-ray charge-coupled device (CCD) detector. Detector orientation relative to the incident beam was calibrated using a diffraction standard (CeO_2) and the detector-sample distance was determined by matching the observed ambient *d*-values of the sample inside the D-DIA to those reported by *Sasaki et al.* [1982]. The sample length was measured by radiography using a wide X-ray beam, by driving the WC slits out of the beam path. The cell assembly used in the present study was similar to that described by *Uchida et al.* [2004]. We used a pre-sintered, fully densified polycrystalline cylindrical specimen (0.8 mm in diameter and 1.2 mm in length), synthesized at 20 GPa and 1523 K using Orange-3000 (Kawai-type apparatus) at Geodynamics Research Center, Ehime University.

[6] Data reported here were collected from a single run, in which five shortening-lengthening deformation cycles

---

[1]Center for Advanced Radiation Sources, University of Chicago, Chicago, Illinois, USA.
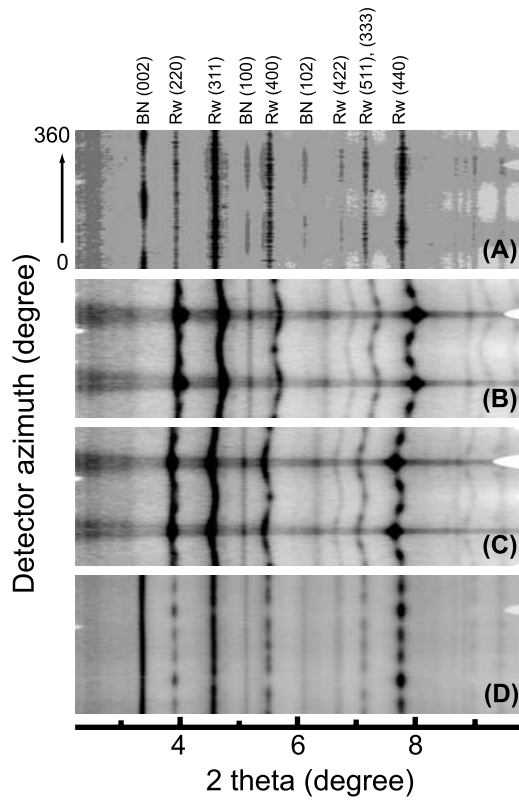[2]Geodynamics Research Center, Ehime University, Matsuyama, Japan.

Figure 1. Representative X-ray diffraction patterns for polycrystalline ringwoodite. (a) Starting material at ambient conditions, (b) $P = 9.7 \pm 0.6$ GPa and $t = 4.6 \pm 0.2$ GPa during shortening with $\langle \dot{\varepsilon} \rangle = 4.7 \pm 0.1 \times 10^{-6}$ s^{-1}, (c) P = 6.4 ± 0.8 GPa and $t = -4.0 \pm 0.1$ GPa during lengthening with $\langle \dot{\varepsilon} \rangle = -3.7 \pm 0.1 \times 10^{-6}$ s^{-1}, (d) recovered sample at ambient conditions.

were carried out at a ram load of 30 T, and four more cycles at 50 T, by advancing and retracting the differential ram pistons at various speeds. In each cycle, an average strain rate ($\langle \dot{\varepsilon} \rangle$) was calculated based on sample length measurements during deformation, beyond the yield point. The corresponding sample strain rates varied by a factor of about twelve.

[7] Methods of data analysis were similar to those described by *Uchida et al.* [2004]. We first determine lattice strain, $\varepsilon\,(\varphi, hkl) = [d_0(\varphi, hkl) - d(\varphi, hkl)]/d_0(\varphi, hkl)$, where φ is the true azimuth angle, given by $\sin\varphi = \cos\theta\sin\chi$ (θ and χ are the diffraction angle and detector azimuth), and $d_0(\varphi, hkl)$ and $d(\varphi, hkl)$ are d-values of the sample at ambient conditions and at a certain pressure and stress state, respectively. Four reflections, (220), (311), (400), and (440), are used in our analysis. The lattice strain, $\varepsilon(\varphi, hkl)$, is fitted to $\varepsilon(\varphi, hkl) = \varepsilon_P - \varepsilon_t(hkl)(1 - 3\sin^2 \varphi)$ to obtain hydrostatic (ε_P) and differential ($\varepsilon_t(hkl)$) lattice strains. The hydrostatic pressure is calculated using ε_P and the third-order Birch-Murnaghan equation of state of ringwoodite [*Meng et al.*, 1994]. We infer the sample differential stress ($t = \sigma_1 - \sigma_3$, where σ_1 and σ_3 are the principal stresses in the vertical and horizontal directions, respectively) by averaging differential stresses calculated from all available reflections hkl: $t(hkl) = \varepsilon_t(hkl)\mathrm{E}(hkl)$, where $\mathrm{E}(hkl)$ is the single-crystal Young's modulus along the given orientation [*Uchida et al.*, 2004;

Weidner et al., 2004]. *Uchida et al.* [2004] have demonstrated that this approach has yielded stress-strain relations similar to those obtained in a conventional deformation experiments for MgO. We used ambient single-crystal elastic moduli determined by *Weidner et al.* [1984] and the pressure derivatives by *Sinogeikin and Bass* [2001], assuming that the small amount of Fe (9%) present in the latter study does not affect the derivatives. The total sample axial strain is calculated using $\varepsilon_{\mathrm{total}} = (l_0 - l)/l_0$, where l is the sample length measured during deformation, and the choices of the reference length l_0 are discussed below.

3. Results and Discussion

[8] Representative X-ray diffraction patterns, converted from the original form in polar coordinates into Cartesian systems, are shown in Figure 1, where the horizontal and vertical axes are 2θ and detector azimuth χ ($\chi = 0$ is parallel to σ_3), respectively, with intensity represented by darkness. In Figure 1a (ambient; stress free), the positions of each diffraction line exhibit no χ dependence, indicting no residual stress in the starting sample. There is also no intensity variation with χ, indicating no preferred orientation. Figures 1b and 1c are patterns collected during shortening and lengthening of the first cycle at 50 T, respectively. Here the peak position of every diffraction line clearly varies with χ. The maxima in 2θ angles at $\chi \sim$ 90 and 270° in Figure 1b correspond to the direction of the compressive principle stress σ_1, with $\sigma_1 > \sigma_3$, where the sample underwent axial shortening. The minima in 2θ at $\chi \sim 90$ and 270° in Figure 1c correspond to $\sigma_1 < \sigma_3$, under which condition the sample underwent axial lengthening. Intensity variation with χ can also be clearly observed in Figures 1b and 1c. For example, intensities of the (440) peak show maxima at $\chi = 30, 90, 150, 210, 270$, and 330°, with well developed six-fold symmetry. These observations have been used to determine texture development in ringwoodite during deformation. Based on this analysis, the deformation is dominated by the $\{111\}\langle-110\rangle$ slip system. Details of the analysis will be reported in a separate paper (H.-R. Wenk et al., Texture development and deformation mechanisms in ringwoodite, manuscript in preparation, 2005). Figure 1d is a diffraction pattern collected from the recovered sample. No χ-dependence in peak positions is observed, indicating that stress has been completely released. Figures 2a and 2b show selected stress-strain curves at 30 and 50 T, respectively. Here, l_0 is chosen to be the length at the beginning of the first deformation cycle under each ram load. For clarity, only the stresses determined from the (311) reflection are shown; other reflections show very similar behavior. A clear hysteresis behavior is observed from these curves. Ringwoodite is readily deformed in ductile regime even at room temperature. There is no evidence for fracture, such as a sudden drop of differential stress or sample length, during the deformation.

[9] In order to examine more closely the stress-strain behavior, we decompose the curves into individual shortening and lengthening segments, and redefine l_0 for each segment as the point where t is zero. It was necessary to perform interpolation in most cases to find the appropriate l_0. Figures 3a and 3b show curves for (311) after l_0 has been redefined. There are ten independent stress-strain curves at 30 T, and eight at 50 T, with solid and open symbols
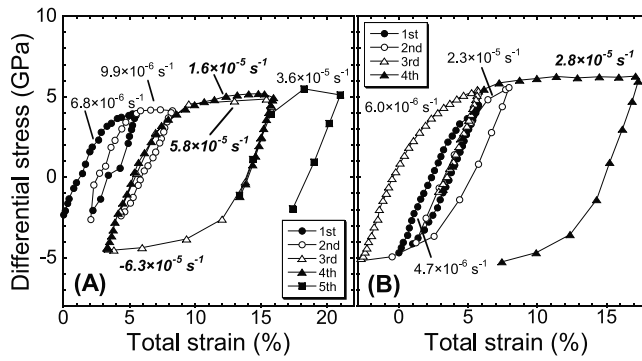
Figure 2. Representative stress-strain curves of ringwoodite at (a) 30 and (b) 50 T. Stresses were determined using the (311) reflection and the reference sample length (l_0) is chosen to be the length at the beginning of the first deformation cycle under each ram load. Strain rates ($\langle \dot{\varepsilon} \rangle$) of some deformation segments are shown: numbers represented by bold italic are average strain rates when the sample exhibits steady-state flow; the others are average strain rates throughout whole deformation segment (from elastic to plastic).

representing data in shortening and lengthening, respectively. These curves are a good representative of the entire sample because the values of differential stresses determined using (311) are essentially identical to the average stresses determined by three major independent reflections of (311), (400), and (440) (see insets in Figures 3a and 3b).

[10] In Figures 3a and 3b, all stress-strain curves exhibit a consistent trend. Stresses vary linearly with strain until $|\varepsilon_{total}|$ reaches about 1.5%, where curves start deviating from linearity. We define this point as the yield point [*Uchida et al.*, 2004]. Below the yield point, ringwoodite deforms in the elastic regime, where all of the data points fall in a well-defined straight line. Beyond the yield point, the differential stress versus strain relation exhibits a strong non-linearity, indicating strain-hardening. Eventually, stresses are saturated when $|\varepsilon_{total}| > 8\%$. We refer to the stress after the attainment of steady-state flow as the ultimate strength.

[11] The data points collected in the plastic regime show a range of stresses, which can be attributed to effects of pressure and total strain in different deformation cycles. Figure 4 shows stresses at selected sample strains (2, 5, and 10%) as a function of pressure. These stresses increase with pressure and axial strain, until the ultimate strength is reached. Changing strain rate from 5×10^{-5} to $4 \times 10^{-6}\ \mathrm{s}^{-1}$ has little effect on the ultimate strength under these conditions (see Figures 2 and 3), suggesting that deformation occurs in the low temperature plasticity regime at these pressure and temperature conditions [*Frost and Ashby*, 1982]. Both shortening and lengthening data show a consistent trend. Thus we conclude that stress-strain curves can be reproduced by repeated cycles at various pressures in a single experiment.

[12] Several previous studies reported high-pressure strengths of polycrystalline ringwoodite at room temperature [*Meade and Jeanloz*, 1990; *Chen et al.*, 1998; *Kavner and Duffy*, 2001]. There is a large discrepancy among the reported values, which may be attributed to grain size, strain

rate, and total strain [*Kavner and Duffy*, 2001]. In those studies, both strain and strain rate were not controlled parameters and could not be measured. Our results, obtained in the D-DIA where differential stress, total strain, and strain rates are controllable and measurable, show that ringwoodite deforms with significant strain hardening at high pressures, before reaching the ultimate strength.

[13] The inset of Figure 4 compares differential stresses measured in this study with those reported in previous studies. The data of *Meade and Jeanloz* [1990] were based on characterizing pressure gradients in the DAC. Their stress levels are much higher than those determined by all other studies, including this study. Possible reasons for this discrepancy have already been discussed by *Kavner and Duffy* [2001]. The trend of our data at 10% strain, where steady state flow was observed, is in general agreement with the DAC results of *Kavner and Duffy* [2001], using the
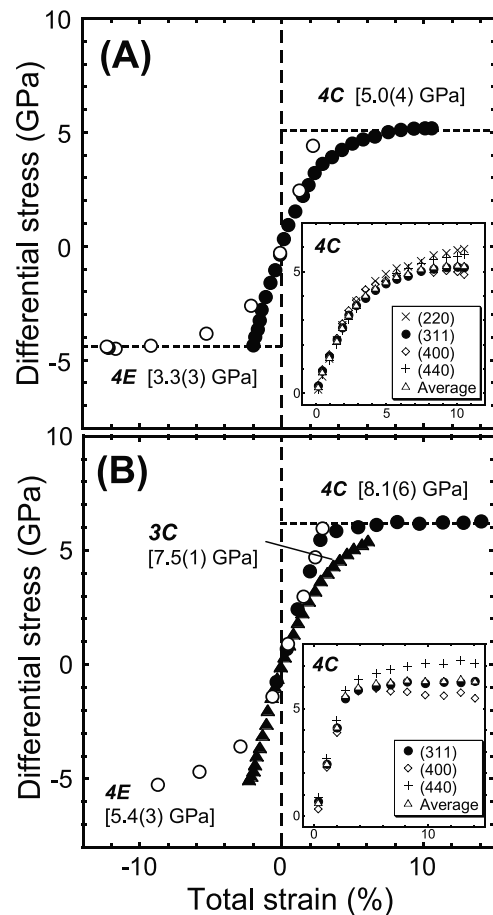

Figure 3. Representative decomposed stress-strain curves of ringwoodite at (a) 30 and (b) 50 T. Stress was determined using the (311) reflection. Each curve is labeled by a numeric followed by a letter. For example, 4C and 4E represents the 4th shortening and lengthening segments, respectively. Solid and open symbols represent data points collected in shortening and lengthening, respectively. Numbers in the parentheses represent average hydrostatic pressures above 5% total strain. Insets show stress-strain curves of the fourth compression at each ram load; stresses were determined using all of usable reflections. Error bars are smaller than the size of the symbols.
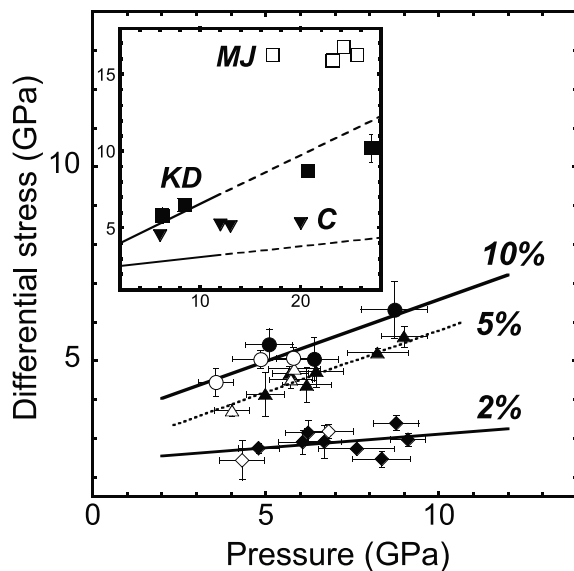
Figure 4. Pressure and strain dependence of differential stress of ringwoodite. The present data are represented at three selected strains: 2% (diamonds), 5% (triangles) and 10% (circles). Closed and open symbols indicate data from compression and extension cycles, respectively. Solid lines represent linear least-square fits of data at 2 and 10%; the dotted line is a guide to the eye for the 5% data. Error bars for pressure and differential stress represent one standard deviations of those determined from the different reflections. The inset compares results with previous studies: MD, *Meade and Jeanloz* [1990]; C, *Chen et al.* [1998]; KD, *Kavner and Duffy* [2001]. Dashed lines in the inset are extrapolations of the linear fits of the present results at 2 and 10% total strain.

radial X-ray diffraction technique [e.g., *Singh et al.*, 1998], similar to our methodology. On the other hand, stresses determined by *Chen et al.* [1998] agree with our data that are between 2 and 5% strain. A T-cup apparatus was used in their study, where stresses were generated by grain-to-grain contact in compressing of a powdered sample and determined by the broadening of diffraction line widths. It appears that the total strain generated in their samples was limited and hence ultimate strength was not achieved.

[14] Flow laws of solids in power-law creep regime, considered one of the major deformation mechanism in the mantle conditions, are commonly described by relations in the form of $\dot{\varepsilon} = A\ \sigma^n \exp(-(E + PV^*)/RT)$, where A is a constant, $\dot{\varepsilon}$ imposed strain rate, σ sample stress, P the hydrostatic pressure, R the gas constant, T the absolute temperature, and n the stress exponent. E and V* are activation energy at room pressure and activation volume, respectively. Once these parameters are determined, the effective viscosity ($\eta = \sigma/2\dot{\varepsilon}$) of the mineral can be calculated at various conditions. In order to derive this constitutive relation experimentally, stress and strain must be measured simultaneously. As we are interested in understanding large strain deformation processes in the Earth, steady-state flow

has to be achieved in the experiment, requiring considerable amounts of strain to be generated. We have demonstrated here that the D-DIA is capable of generating steady-state flow in the sample while allowing us to measure stress-strain curves at high pressures with controlled strain rates. Thus, quantitative flow laws can be determined using this technique.

References

Chen, J., T. Inoue, D. J. Weidner, Y. Wu, and M. T. Vaughan (1998), Strength and water weakening of mantle minerals, olivine, wadsleyite and ringwoodite, *Geophys. Res. Lett.*, 25, 575–578.

Frost, H. J., and M. F. Ashby (1982), *Deformation-Mechanism Maps*, pp. 108–110, Elsevier, New York.

Irifune, T., and A. E. Ringwood (1987), Phase transformations in a harzburgite composition to 26 GPa: Implications for dynamical behaviour of the subducting slab, *Earth Planet. Sci. Lett.*, 86, 365–376.

Karato, S., C. Dupas-Bruzek, and D. C. Rubie (1998), Plastic deformation of silicate spinel under the transition-zone conditions of the Earth's mantle, *Nature*, 395, 266–296.

Kavner, A., and T. S. Duffy (2001), Strength and elasticity of ringwoodite at upper mantle pressures, *Geophys. Res. Lett.*, 28, 2691–2694.

Meade, C., and R. Jeanloz (1990), The strength of mantle silicate at high pressures and room temperature: Implications for the viscosity of the mantle, *Nature*, 348, 533–535.

Meng, Y., Y. Fei, D. J. Weidner, G. D. Gwanmesia, and J. Hu (1994), Hydrostatic compression of γ-Mg_2SiO_4 to mantle pressures and 700 K: Thermal equation of state and related thermoelastic properties, *Phys. Chem. Miner.*, 21, 407–412.

Sasaki, S., C. T. Prewitt, Y. Sato, and E. Ito (1982), Single-crystal X-ray study of gamma-Mg_2SiO_4, *J. Geophys. Res.*, 87, 7829–7832.

Singh, A. K., H.-K. Mao, J. Shu, and R. J. Hemley (1998), Estimation of single-crystal elastic moduli from polycrystalline X-ray diffraction at high pressure: Application to FeO and iron, *Phys. Rev. Lett.*, 80, 2157–2160.

Sinogeikin, S. V., and J. D. Bass (2001), Single-crystal elasticity of g-$(Mg_{0.91}Fe_{0.09})_2SiO_4$ to high pressures and to high temperatures, *Geophys. Res. Lett.*, 28, 4335–4338.

Uchida, T., Y. Wang, M. L. Rivers, and S. R. Sutton (2004), Yield strength and strain hardening of MgO up to 8 GPa measured in the deformation-DIA with monochromatic X-ray diffraction, *Earth Planet. Sci. Lett.*, 226, 117–126.

Wang, Y., W. B. Durham, I. C. Getting, and D. J. Weidner (2003), The deformation-DIA: A new apparatus for high temperature triaxial deformation to pressures up to 15 Gpa, *Rev. Sci. Instrum.*, 74, 3002–3011.

Weidner, D. J., H. Sawamoto, S. Sasaki, and M. Kumazawa (1984), Single-crystal elastic properties of the spinel phase of Mg_2SiO_4, *J. Geophys. Res.*, 89, 7852–7860.

Weidner, D. J., L. Li, M. Davis, and J. Chen (2004), Effect of plasticity on elastic modulus measurements, *Geophys. Res. Lett.*, 31, L06621, doi:10.1029/2003GL019090.

Wenk, H.-R., I. Lonardelli, J. Pehl, J. Devine, V. Prakapenka, G. Shen, and H.-K. Mao (2004), In situ observation of texture development in olivine, ringwoodite, magnesiowüstite and silicate perovskite at high pressure, *Earth Planet. Sci. Lett.*, 226, 507–519.

———————————

T. Irifune, Geodynamics Research Center, Ehime University, 2-5 Bunkyo-cho, Matsuyama 790-8577, Japan. (irifune@dpc.ehime-u.ac.jp)

N. Nishiyama, M. L. Rivers, S. R. Sutton, T. Uchida, and Y. Wang, Center for Advanced Radiation Sources, University of Chicago, 5640 South Ellis Avenue, Chicago, IL 60637, USA. (nishiyama@cars.uchicago.edu; rivers@cars.uchicago.edu; sutton@cars.uchicago.edu; uchida@cars.uchicago.edu; wang@cars.uchicago.edu)